

Origin of the negative temperature coefficient of resistivity in the half-Heusler antimonides LuNiSb and YPdSb

Daniel Gnida , Kamil Ciesielski , and Dariusz Kaczorowski 

Institute of Low Temperature and Structure Research, Polish Academy of Sciences, P.O.Box 1410, 50-950 Wrocław, Poland

 (Received 27 January 2021; revised 24 March 2021; accepted 30 April 2021; published 19 May 2021)

The electrical transport in the half-Heusler phases LuNiSb and YPdSb was measured in a temperature range 2–300 K. For both compounds, the electrical resistivity was found to decrease with increasing temperature, showing a linear-in- T behavior over an extended temperature interval. In order to interpret the experimental data, a two-channel conductivity model was applied, which revealed that not only the semiconducting-like transport but also the metallic-like one exhibit negative temperature coefficients. The unusual behavior in the metallic channel was described within the Cote-Meisel formalism based on the diffraction model of strongly disordered metals. In addition, a weak localization scenario was considered including spin-orbit scattering and Coulomb interaction between conducting electrons. The electron-electron interaction was found most important at the lowest temperatures, where the semiconducting channel becomes ineffective, reminiscent of charge transport confined to a narrow yet finite-size metallic band located inside the semiconducting energy gap. The low-temperature resistivity of YPdSb appeared fully describable in terms of the Altshuler-Aronov quantum correction due to interacting electrons. In turn, the electronic transport in LuNiSb was found affected by the Kondo effect associated with a small amount of paramagnetic impurities present in the specimen investigated. The approach developed for LuNiSb and YPdSb can be applied to other half-Heusler compounds that exhibit atom disorder in their crystal structures.

DOI: [10.1103/PhysRevB.103.174206](https://doi.org/10.1103/PhysRevB.103.174206)

I. INTRODUCTION

Searching for new highly efficient and clean energy-conversion systems is an important challenge in a global sustainable energy solution. An application of thermoelectric (TE) materials based devices allowing to convert directly heat into electricity and vice versa is one of the future-oriented developments, which could contribute to significant progress in this area. Therefore, for many years, scientific research and industrial sectors have been aimed at achieving more and more efficient thermoelectrics.

The maximum possible performance of a TE device at a given temperature is determined by the so-called thermoelectric figure of merit, ZT , the magnitude of which depends on the intrinsic charge and heat transport characteristic of the material used, namely, its electrical conductivity, thermal conductivity and thermoelectric power [1]. These properties are fundamentally interrelated, and each of them depends on mechanisms of charge conduction and its dissipation. Hence, thorough understanding of the electronic transport in potential candidates for TE applications is vital for the optimization of TE material performance.

In this work, we investigated the mechanisms of charge conduction in YPdSb [2] and LuNiSb [3,4]. Both compounds belong to a group of half-Heusler (HH) phases, intensively studied due to their promising TE properties [5–8]. An inherent feature of the HH compounds is crystallographic disorder and its strong influence on their physical properties [9–14]. In particular, with changing the degree of structural disorder,

the electrical conductivity in these materials can vary from narrow-gap semiconducting to metallic-like behavior [9].

Alike many other HH compounds [4,15–17], LuNiSb and YPdSb exhibit a negative temperature coefficient of the electrical resistivity (TCR) [2–4]. Commonly, the negative sign of TCR in such HH materials is interpreted as an indication of the presence of a narrow gap in their electronic band structure of the order of 100 meV [18–21]. It should be noted, however, that the temperature dependencies of the electrical resistivity $\rho(T)$ of YPdSb and LuPdSb do not show any exponential behavior over an extended temperature interval, usually expected for simple semiconductors [2–4]. This feature hints at more complex conductivity mechanism. Previously, some attempts were made to account for the experimental $\rho(T)$ variations of the two antimonides by considering multiple energy gaps [15] or incorporating additional conduction channels of metallic or insulating type [2,16]. Though those approaches led to better mathematical description of $\rho(T)$, it remains unclear what is the actual electronic ground state in these ternaries and what is the origin of their negative TCR. Remarkably, the electrical resistivity of both materials comprises a distinct linear or quasilinear contribution, and its origin is also ambiguous.

To address those open issues, we performed detailed analysis of the electronic transport in YPdSb and LuNiSb, focusing at the role of disorder in their crystal structure. We established that the structural disorder not only influences their electronic structure but also leads to emergence of additional conduction channels, the presence of which explains negative TCR. The

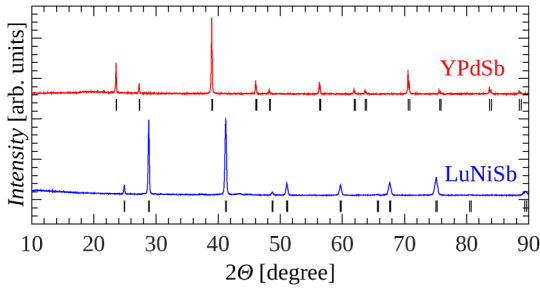


FIG. 1. Powder XRD patterns of LuNiSb and YPdSb. Vertical ticks mark the Bragg peaks positions.

present work constitutes a part of larger project aimed at understanding magneto-transport properties of rare-earth based HH phases [22–28].

II. EXPERIMENTAL

Polycrystalline specimens of LuNiSb and YPdSb were synthesized by arc-melting constituent elements (purity Y, Lu 99.9 at.%, Ni 99.999 at.%, Pd 99.99 at.%, and Sb 99.999 at.%) in Ti-gettered argon atmosphere. The ingots were flipped over and remelted several times to promote homogeneity. Both samples were annealed at 800 °C for 14 days. In the case of LuNiSb, however, the thermal treatment resulted in occurrence of nickel-rich precipitations, so for the study of transport properties the as-cast sample was chosen.

Phase purity was checked by powder x-ray diffraction (XRD) performed at room temperature using a PANanalytical diffractometer (Cu K_α radiation, $\lambda = 1.5406$ Å). The obtained XRD patterns of YPdSb and LuNiSb (Fig. 1) were easily indexed using the FULLPROF program [29] assuming a cubic crystal structure of the MgAgAs-type. The so-derived lattice parameters: $a = 6.532$ Å for YPdSb and $a = 6.198$ Å for LuNiSb, are close to those reported in the literature [30,31]. No foreign Bragg peaks were found.

Magnetotransport measurements were carried out in the temperature range 2–300 K and in external magnetic fields up to 9 T employing standard ac four-point technique implemented in a Quantum Design PPMS-9 platform. Bar-shaped specimens were cut using a wire saw, and electrical leads were attached to them with a silver epoxy paste. Numerical analyses of the experimental data were performed by means of the TABLECURVE 2D software [32].

III. RESULTS

The temperature variations of the electrical resistivity of LuNiSb and YPdSb are displayed in Figs. 2(a) and 2(b), respectively. For both compounds, the resistivity changes with decreasing temperature in a very similar manner, reported also for other HH intermetallics [4,15,16]. Below 300 K, $\rho(T)$ exhibits a quasilinear increase, while at the lowest temperatures, a distinct rise in the slope of the resistivity curve is observed. In the case of LuNiSb, those two characteristic regimes are separated by a crossover region in which $\rho(T)$ shows clear tendency towards flattening. In turn, for YPdSb, such a crossover behavior is hardly pronounced.

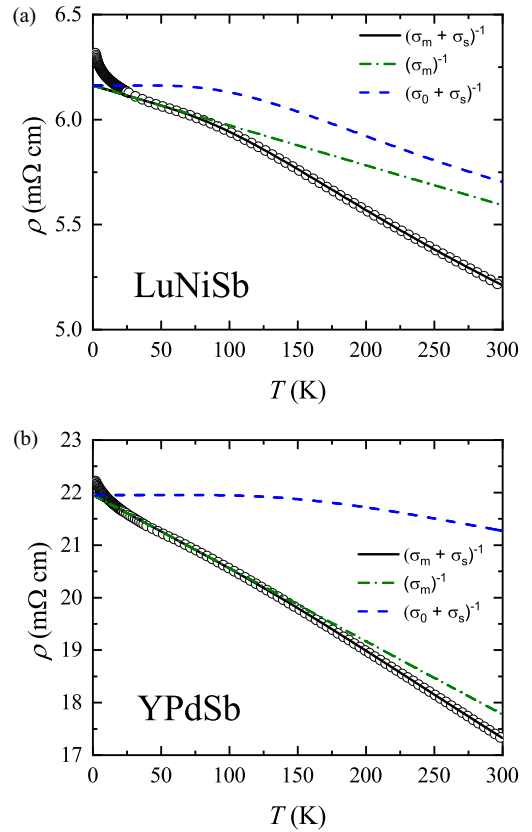


FIG. 2. Temperature dependence of the electrical resistivity of (a) LuNiSb and (b) YPdSb. Solid lines represent the least-squares fitting of Eq. (1) to the experimental data above 50 K. Dashed and dash-dotted lines correspond to the curves calculated with $a = 0$ and $\sigma_a = 0$, respectively. Presented in the legend parameter $\sigma_0 = \rho_0^{-1}$.

A. Two-channel conductivity model

In order to model the experimental $\rho(T)$ data of LuNiSb and YPdSb, two parallel conductivity channels were considered, namely, metallic-like (σ_m) and semiconducting-like (σ_s):

$$\rho = (\sigma_m + \sigma_s)^{-1} \quad (1)$$

represented by the formulas

$$\sigma_m = (\rho_0 + aT)^{-1}, \quad (2)$$

$$\sigma_s = \sigma_a \exp\left(\frac{-E_g}{2k_B T}\right), \quad (3)$$

where ρ_0 stands for the residual resistivity, aT can be a simple approximation of electron-phonon scattering contribution, and E_g denotes a semiconducting energy gap. Fitting the experimental data above 50 K with the function given by the above equations yielded the parameters: $\sigma_a = 0.051 (\text{m}\Omega \text{ cm})^{-1}$, $\rho_0 = 6.16 \text{ m}\Omega \text{ cm}$, $a = -0.0019 \text{ m}\Omega \text{ cm K}^{-1}$, $E_g = 70 \text{ meV}$ for LuNiSb, and $\sigma_a = 0.013 (\text{m}\Omega \text{ cm})^{-1}$, $\rho_0 = 21.96 \text{ m}\Omega \text{ cm}$, $a = -0.014 \text{ m}\Omega \text{ cm K}^{-1}$, $E_g = 120 \text{ meV}$ for YPdSb. The so-estimated energy gaps are similar to those determined in the previous experimental studies and calculated for these compounds from the first principles [2,4,19].

As can be inferred from Fig. 2, both components in Eq. (1) give significant contribution to the overall temperature dependence of the electrical resistivity of LuNiSb, while $\rho(T)$ of YPdSb is governed mostly by the metallic channel. Another finding is that the exponential increase in the resistivity in the semiconducting channel is entirely cut off at temperatures below 80 K for LuNiSb and 120 K for YPdSb. In those low-temperature regions, the electronic transport is principally determined by the metallic conduction, governed mostly by scattering conduction electrons on the structural defects (see below).

The most peculiar result of the performed analyses is the negative sign of the coefficient a obtained for both materials. This finding clearly indicates that the phonon contribution to their electrical transport cannot be accounted for within a simple Bloch-Grüneisen approach, and thus the linear-in- T term in Eq. (2) must have a different origin. As mentioned in the Introduction, a natural source of negative TCR in the HH phases can be crystallographic disorder, inherent to many of them [10,13,33]. According to the Mooji rule [34], in disordered metallic systems, the resistivity magnitude and the sign of TCR strongly depend on the degree of atomic disorder. Furthermore, in some cases, the negative TCR can take a form of linear or quasilinear $\rho(T)$, as observed for LuNiSb and YPdSb.

B. Cote-Meisel model

One of the concepts often used in describing the electrical transport in disordered metallic systems is based on the generalized Faber-Ziman diffraction model, originally predicted for liquid alloys [35]. The approach was developed for amorphous systems, like glassy NiP [36], and assumes that their resistivity is mainly governed by structure factors. In the frame of the Cote and Meisel approximation [37], $\rho(T)$ of highly resistive metals, both crystalline and amorphous, can be described by the relation

$$\rho \cong (1 - \gamma)\rho_{ip} + \rho_0 e^{-2W}. \quad (4)$$

The first term represent an ideal single-phonon resistivity, which is reduced by a factor $(1 - \gamma)$ due to ineffective scattering of conduction electrons with a wavelength larger than mean free path. The second contribution corresponds to an elastic component of the resistivity that takes into account the effect of thermal vibrations on elastic structure factor by including Debye-Waller damping term e^{-2W} . Here, W is an average Debye-Waller exponent with the temperature dependence given by the relation [38]:

$$W(T) = \frac{3\hbar^2 \langle k^2 \rangle T^2}{2Mk_B \Theta_D^3} \int_0^{\Theta_D/T} \left(\frac{1}{e^z - 1} + \frac{1}{2} \right) z dz \quad (5)$$

where \hbar denotes the reduced Planck constant, k_B stands for the Boltzmann constant, Θ_D corresponds to the Debye temperature, k is the scattering wave vector of conduction electrons, and M is the molar mass. The bracket $\langle \rangle$ denotes averaging over the scattering vectors k at the Fermi energy. It can be shown that for small values of the Debye-Waller exponent, the elastic scattering term is a linear function of temperature for $T > \Theta_D/2$, while at lower temperatures $T < \Theta_D/2$, it transforms into a T^2 dependence.

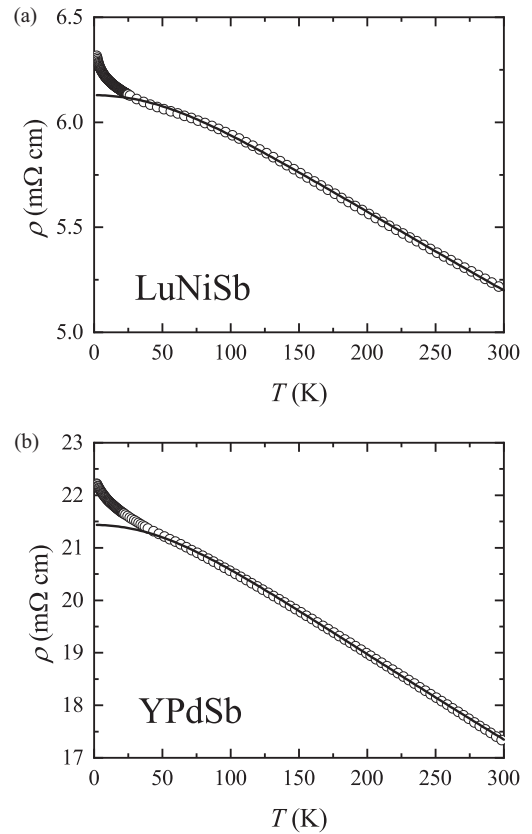


FIG. 3. Temperature dependence of the electrical resistivity of (a) LuNiSb and (b) YPdSb. Solid lines represent the fitting of Eq. (4) to the high-temperature experimental data.

In the analyses of the experimental $\rho(T)$ data of LuNiSb and YPdSb in terms of Eq. (4), the single-phonon term was neglected as both compounds showed negative TCR in the entire temperature range investigated. Moreover, the fitting was done at high temperatures only (for $T > 100$ K), and thus a linear-in- T asymptotic form of W was assumed. With these restrictions, the Cote-Meisel model was found to represent the measured data of both compounds reasonably well (see solid lines in Fig. 3). Clearly, the agreement between the experimental and calculated resistivity curves is not worse than that obtained using the two conduction channel model in a similar temperature interval. As a result of the Cote-Meisel approach, the following parameters were derived: $\rho_0 = 6.5$ m Ω cm, $\langle k^2 \rangle = 8.53 \times 10^{20}$ m $^{-2}$, $\Theta_D = 349$ K for LuNiSb, and $\rho_0 = 23.3$ m Ω cm, $\langle k^2 \rangle = 9.16 \times 10^{20}$ m $^{-2}$, $\Theta_D = 350$ K for YPdSb. Remarkably, the so-derived Debye temperature of LuNiSb matches very well with Θ_D obtained from the heat capacity data [4]. In turn, the Debye temperature estimated for YPdSb is somewhat larger than the value determined by means of the heat capacity experiment ($\Theta_D = 275$ K) [2]. The value of $\langle k^2 \rangle$ is usually of the order of k_F^2 , where k_F stands for the Fermi wave vector. In disordered metallic systems, $2k_F$ scattering processes dominate the electrical transport, so one can assume that $\langle k^2 \rangle = (2k_F)^2$. From the latter relation, within the framework of free electron model with spherical Fermi surface, the Fermi wave vector is estimated to about 1.5×10^{10} m $^{-1}$ for both compounds studied.

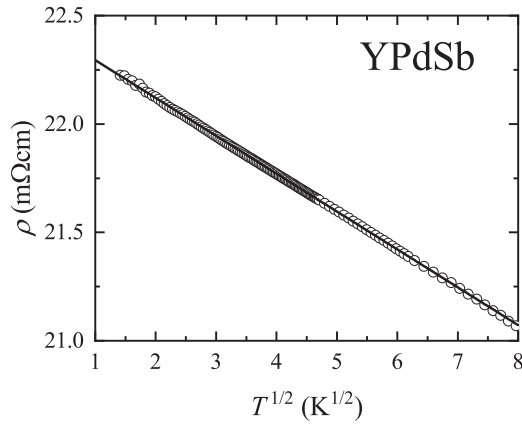


FIG. 4. Low-temperature electrical resistivity of YPdSb as a function of square-root of temperature. Solid line is a least-squares fit of Eq. (6) to the experimental data below 60 K.

Then, using the values of the Sommerfeld coefficient reported in Refs. [2,4], one can calculate the effective masses of charge carriers in LuNiSb and YPdSb to be roughly $m_{\text{eff}} = 0.5m_e$ and $0.05m_e$, respectively.

C. Electron-electron interaction and weak localization

The analysis of the electrical transport in LuNiSb and YPdSb in terms of the Cote-Meisel model was applied to the resistivity data measured above 100 K. At lower temperatures, $\rho(T)$ of these compounds does not level off as one would expect for simple metals. Instead, the resistivity continues to increase with decreasing temperature, however with a local TCR larger than the slope of the linear-in- T dependence seen at high temperatures. Remarkably, the upturn in $\rho(T)$ could not be described by the Mott relation $\rho \propto [\exp(1/T)]^{1/4}$ (Ref. [39]), characteristic of insulating systems with charge hopping (not shown). Instead, as visualized in Fig. 4, the low-temperature resistivity of YPdSb can be approximated by the relation [40]

$$\rho(T) = \rho_0 + AT^{1/2}, \quad (6)$$

predicted for disordered metallic systems with strong electron-electron Coulomb interaction represented by the parameter A . Fitting this so-called Altshuler-Aronov (AA) correction to the resistivity of YPdSb measured below 60 K, yielded the parameters $\rho_0 = 22.5 \text{ m}\Omega \text{ cm}$ and $A = -0.17 \text{ m}\Omega \text{ cm K}^{-1/2}$.

In contrast to YPdSb, $\rho(T)$ of LuNiSb does not follow the simple $T^{1/2}$ relation [see Fig. 5(a)], which suggests the presence of another mechanism of conduction electron scattering. Remarkably, this additional contribution to the resistivity can be suppressed by applying external magnetic field, and in strong enough magnetic fields the pure AA behavior was found. Though the origin of this extra contribution to $\rho(T)$ of LuNiSb is unknown, it is worth recalling that very similar temperature dependencies of the electrical transport studied in zero and finite magnetic field was observed before for a sample of structurally disordered intermetallic silicide La_2NiSi_3 that contained small amount of paramagnetic impurities [41]. In the case of LuNiSb, application of Eq. (6) to the

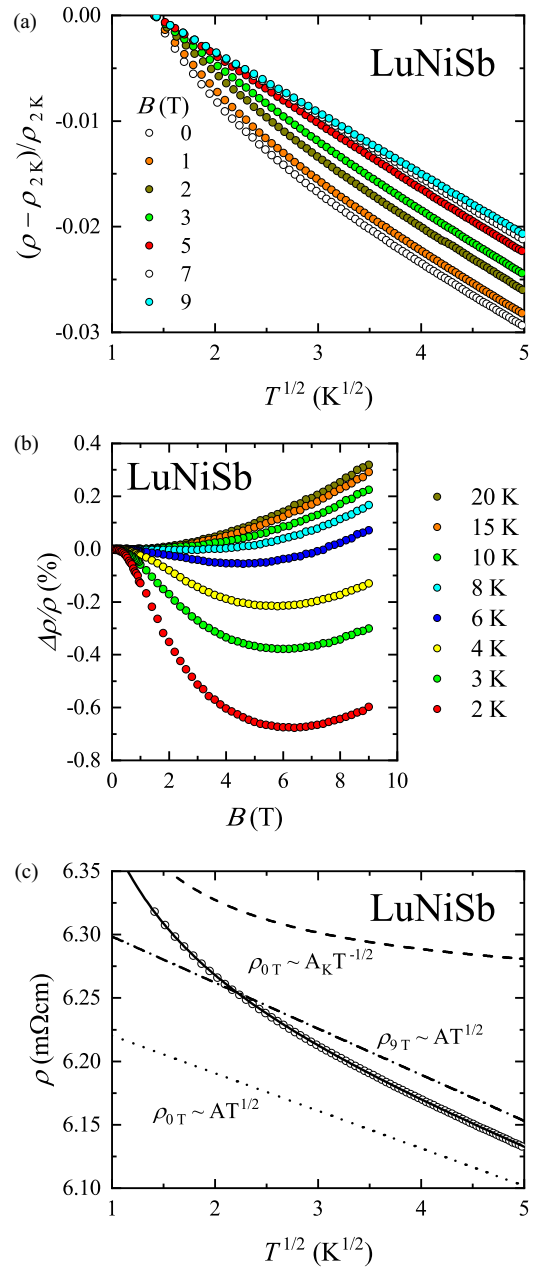


FIG. 5. (a) Low-temperature electrical resistivity of LuNiSb, normalized to its value at $T = 2 \text{ K}$, measured in different external magnetic fields and plotted as a function of square-root of temperature. (b) Magnetic field variations of the transverse magnetoresistance of LuNiSb taken at different temperatures. (c) Zero-field low-temperature electrical resistivity of LuNiSb plotted as a function of $T^{1/2}$. Solid line is a least-squares fit of Eq. (7) to the experimental data below 25 K. The AA and Kondo contributions are represented by dotted and dashed lines, respectively. For comparison, the resistivity data of LuNiSb measured in magnetic field of 9 T is shown by dash-dotted line.

experimental data measured below 25 K in fields $B > 5 \text{ T}$ gave the fitting parameters $\rho_0 = 6.33 \text{ m}\Omega \text{ cm}$ and $A = -0.04 \text{ m}\Omega \text{ cm K}^{-1/2}$, which are comparable to those of YPdSb.

Figure 5(b) displays the transverse magnetoresistance (MR) isotherms of LuNiSb expressed as $\Delta\rho/\rho = (\rho(B) - \rho(0))/\rho(0)$. At temperatures $T \leq 4$ K, MR is negative in the entire magnetic field range examined. A characteristic feature of these curves is a broad minimum that occurs near 6 T at $T = 2$ K, and slightly shifts to smaller fields with rising temperature. At the same time, the magnitude of MR decreases and the minimum gets more and more shallow. The isotherm taken at 6 K exhibits a sign change in strong magnetic fields, and those measured at $T \geq 8$ K show positive MR in the whole field range. The MR data recorded at 20 K can be described using a simple power-law function $\text{MR} \propto B^n$ with the exponent $n \simeq 2$.

The overall behavior of the magnetoresistance of LuNiSb indicates the interplay of at least two contributions with opposite signs. The positive term that dominates MR at high temperatures can be attributed mainly to deflection of charge carriers trajectories under Lorentz force. In addition, in view of the presence of atom disorder in the crystal lattice of the compound (signaled by its large residual resistivity), one can expect additional contributions due to electron-electron interaction or weak localization in the presence of spin-orbit interaction, which both have a form of positive MR with parabolic magnetic field variation in a small field limit of weakly localized regime of moderately disordered metals [40,42]. In turn, the negative contribution to MR of LuNiSb, found at low temperatures in weak magnetic fields, may originate from Kondo effect associated with the contamination of the sample studied by small amount of magnetic impurities, as suggested before for La_2NiSi_3 [41]. In a natural way, application of external magnetic field causes polarization of magnetic moments localized on the impurities, and thus the negative contribution to MR diminishes with increasing the field strength. Usually, the single-ion Kondo interaction yields an additional term in the temperature-dependent resistivity that is proportional to $-\ln T$ [43]. However, as argued in Ref. [44], the presence of paramagnetic impurities may also result in a quantum correction to the electrical conductivity of disordered systems that scales as $T^{-1/2}$. Assuming the latter relationship, the low-temperature resistivity data of LuNiSb was numerically analyzed by the formula

$$\rho(T) = \rho_0 + AT^{1/2} + A_K T^{-1/2} \quad (7)$$

that accounts for the interplay of the AA and Kondo scattering mechanisms. In this equation, which is an extension of Eq. (6) afore-applied for describing the low-temperature resistivity of YPdSb, the parameter A_K is related to the exchange interaction between spin and conduction electrons, the density of states at the Fermi energy, and the elastic scattering time [44]. Fitting Eq. (7) to the $\rho(T)$ data of LuNiSb measured in zero magnetic field below 25 K [see Fig. 5(c)] yielded $A = -0.03 \text{ m}\Omega \text{ cm K}^{-1/2}$, $A_K = 0.155 \text{ m}\Omega \text{ cm K}^{1/2}$, and $\rho_0 = 6.25 \text{ m}\Omega \text{ cm}$. Remarkably, the obtained value of A is close to that determined from $\rho(T)$ measured for LuNiSb in magnetic field of 9 T (cf. above). This finding implies that triplet term in the Coulomb interaction correction hardly contributes to the AA scattering, as usually observed for semiconducting systems [40]. The absence of this term in LuNiSb probably results from spin scattering due to the presence of paramagnetic impurities and/or strong spin-orbit interaction

[45]. Actually, as displayed in Fig. 5(c), the slope of the $T^{1/2}$ term in the zero-field resistivity data slightly differs from the slope of $\rho(T)$ measured in 9 T. This small discrepancy can be tentatively attributed to some additional quantum phenomena related to the electrical conductivity, e.g., the weak localization (WL) effect [46].

A theoretical model that takes into account both the WL contribution including spin-orbit coupling and the Coulomb interaction term was developed in Ref. [47]. In that approach, the total excess resistivity due to the quantum corrections can be expressed as

$$\Delta\rho(T) = -\frac{e^2\rho_0^2}{2\pi^2\hbar} \left(3\sqrt{b + \frac{c}{4}} - \sqrt{\frac{c}{4}} - 3\sqrt{b} + d\sqrt{T} \right), \quad (8)$$

where $b = (D\tau_{\text{so}})^{-1}$, $c = (D\tau_\varphi)^{-1}$, $d = 2.21 \times 10^5 D^{-1/2}$, τ_{so} represents the spin-orbit scattering time, τ_φ stands for the electron dephasing time, and D corresponds to the diffusion coefficient. The first three terms in the bracket are associated with the WL contribution, while the last term corresponds to the afore-discussed electron-electron interaction correction. The WL effect depends on temperature via the temperature variation of τ_φ [48]:

$$\frac{1}{\tau_\varphi(l, T)} = \frac{1}{\tau_\varphi^0(l)} + \frac{1}{\tau_{\text{in}}(l, T)}. \quad (9)$$

In the latter formula, the T -dependent part is primarily associated with inelastic scattering of conduction electrons. Independent on the mechanism which leads to suppression of the quantum interference effect, the inelastic scattering rate takes a form of power law with the exponent equal to 1 or $3/2$ for screened Coulomb interactions [40,49] or to an integer value from the range 2–4 in the case of scattering conduction electrons by phonons [50]. For simplicity, it can be assumed that these different inelastic scattering mechanisms contribute to the overall relaxation process with an average constant β and an effective exponent p , viz.

$$\frac{1}{\tau_\varphi(l, T)} \propto \beta T^p. \quad (10)$$

In order to examine the WL contribution to the electrical transport of LuNiSb and YPdSb, first the semiconducting channel was extracted from the measured $\rho(T)$ data. Shown in Fig. 6 is the metallic-like resistivity of the two compounds, derived using Eq. (1). In the case of LuNiSb, to describe the low-temperature region properly, additional contribution $A_K T^{-1/2}$ was also considered. It should be noticed that the latter term quickly saturates with increasing temperature, and thus hardly affects the high-temperature region of $\rho(T)$. The analysis was performed setting the values of A_K and d equal to those determined in the course of the low-temperature data analysis. Fitting Eq. (8) to the so-treated experimental data yielded the parameters collected in Table I, and results of the analyzes are shown in Figs. 6(a) and 6(b) for LuNiSb and YPdSb, respectively. As evident from these figures, at low temperatures, $\rho_m(T)$, is governed by the electron-electron interaction effect (note dashed lines), and this is because the WL correction (marked by dash-dotted lines) forms a plateau below about 100 and 50 K for LuNiSb and YPdSb, respectively. At higher temperatures, the WL contribution shows a

TABLE I. Parameters obtained for LuNiSb and YPdSb from the analyses of the metallic contribution of the resistivity in terms of Eq. (8). See the main text for the explanation of the symbols.

compound	ρ_0 (m Ω cm)	b (10^{13} m $^{-2}$)	$\beta/(4D)$ (10^7 m $^{-2}$ K $^{-p}$)	p
LuNiSb	6.25	3.87	3.38	2.93
YPdSb	22.5	0.45	4.46	2.74

power-law temperature dependence due to the change in the scattering rate given by Eq. (10). For both compounds, the exponent p was found close to 3, which suggests that the electron dephasing is caused mainly by the inelastic scattering of conduction electrons on longitudinal phonons [50].

IV. DISCUSSION

Ab initio calculations of the electronic band structures of nominally stoichiometric HH phases revealed the presence of a narrow energy gap of the order of tens or hundreds meV, in rough agreement with the values derived from the experimental data [18–21]. However, in most cases, the electrical conductivity in these materials could not be described with a simple exponential function in any extended temperature range, and this finding was associated with the atom disorder in the crystallographic unit cells inherent to the HH

compounds [2–4]. It was shown that the structural disorder strongly influences their physical properties, and in particular, the disorder can result in a change from narrow-gap semiconducting to bad metal behaviors [9].

By the very nature of the disorder, it follows that the structural imperfections, including point defects, are distributed in the crystal lattice in a random way. Recently, it was revealed by means of atomic-resolution imaging that the presence of such disordered defects can bring about some local deviations from the nominal chemical composition [14,25]. In consequence, the macroscopic sample may exhibit diverse electronic properties in regions characterized by slightly different compositions. These findings were supported by the disorder-dependent electronic structure calculations [9].

A straightforward approach to accounting for the disorder-induced inhomogeneity in the transport properties of real specimens of the HH compounds is using a multichannel conduction model. In the simplest scenario, usually adopted in the literature, two conductivity channels are considered, namely, semiconducting-like, with *negative* TCR, and simple metallic-like, characterized by *positive* TCR [2,51]. Remarkably, in the present case of LuNiSb and YPdSb, the two channel model yielded the *negative* slope of the metallic contribution to the measured resistivity, characteristic of disordered metals. Furthermore, this term was found to vary with temperature in a linear fashion within an extended T region. The observed behavior of $\rho(T)$ was described in terms of the interplay of disorder-dependent conduction and quantum effects. At low temperatures, the electronic transport in LuNiSb and YPdSb appeared governed by electron-electron interaction effect, predicted by Altshuler and Aronov for disordered conductors [40]. This situation is analogous to the case of strongly doped semiconductors, in which a narrow metallic band is located inside their semiconducting energy gap, and thus supports the presumption that the key factor influencing $\rho(T)$ of LuNiSb and YPdSb is the randomness in scattering potential.

At this point, it should be recalled that there are known other conductivity mechanisms, not addressed in the present work, which may also contribute to the observation of negative TCR and linear-in- T resistivity behavior [52,53]. In contrast to the WL effect, they focus at strong coupling limit of the electron-phonon interaction, however, in each of them, the structural disorder is an important ingredient. Thus it is rather hardly distinguishable which of these mechanisms are most appropriate for the physical description of the electronic transport properties not only in the HH phases considered in the present work but also in many other disordered systems, characterized by negative TCR and linear or quasilinear temperature dependence of the electrical resistivity in extended temperature interval. Hence, the subject of low-temperature electronic properties in disordered materials is likely to

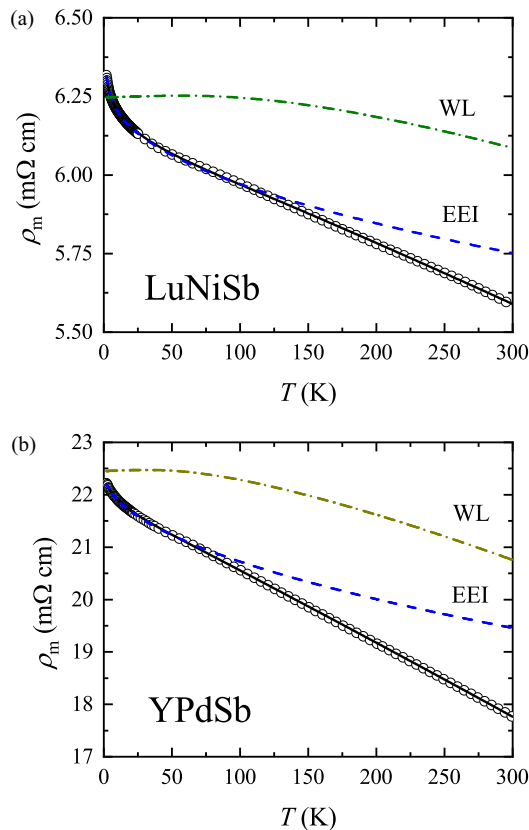


FIG. 6. Temperature variation of the metallic-like electrical resistivity of (a) LuNiSb and (b) YPdSb. Solid lines represent the fits of Eq. (6) to the experimental data. The contributions due to the electron-electron interaction (EEI) and the weak localization (WL) effects are drawn by dashed and dash-dotted lines, respectively.

stimulate further interest from both experimental and theoretical perspectives.

V. CONCLUSIONS

The performed analyzes of the electrical transport in the HH compounds LuNiSb and YPdSb indicated that the negative TCR observed in the entire temperature interval covered (2–300 K) originates from both the semiconducting and metallic conductivity channels. The unusual temperature dependence of the resistivity in the latter channel is governed by the structural disorder. At the lowest temperatures studied,

the semiconducting channel becomes ineffective, and $\rho(T)$ is mostly determined by the metallic contribution, dominated by the electron-electron interaction effect in disordered conducting medium. The approach developed for LuNiSb and YPdSb may appear applicable to other HH phases with disordered crystal structures, where the interplay of semiconducting and atypical metallic conduction is very likely.

ACKNOWLEDGMENT

This work was supported by the National Science Centre (Poland) under research Grant No. 2015/18/A/ST3/00057.

-
- [1] G. J. Snyder and E. S. Toberer, *Nat. Mater.* **7**, 105 (2008).
- [2] K. Gofryk, D. Kaczorowski, T. Plackowski, J. Mucha, A. Leithe-Jasper, W. Schnelle, and Y. Grin, *Phys. Rev. B* **75**, 224426 (2007).
- [3] R. Skolozdra, A. Guzik, A. Goryn, and J. Pierre, *Acta Phys. Pol. A* **92**, 343 (1997).
- [4] K. Ciesielski, K. Synoradzki, I. Wolańska, P. Stachowiak, L. Kępiński, A. Jeżowski, T. Toliński, and D. Kaczorowski, *J. Alloys Compds.* **816**, 152596 (2020).
- [5] L. Huang, Q. Zhang, B. Yuan, X. Lai, X. Yan, and Z. Ren, *Mater. Res. Bull.* **76**, 107 (2016).
- [6] C. Fu, S. Bai, Y. Liu, Y. Tang, L. Chen, X. Zhao, and T. Zhu, *Nat. Commun.* **6**, 8144 (2015).
- [7] M.-S. Lee, F. P. Poudeu, and S. D. Mahanti, *Phys. Rev. B* **83**, 085204 (2011).
- [8] K. Synoradzki, K. Ciesielski, L. Kępiński, and D. Kaczorowski, *J. Appl. Phys.* **123**, 235101 (2018).
- [9] P. Larson, S. D. Mahanti, and M. G. Kanatzidis, *Phys. Rev. B* **62**, 12754 (2000).
- [10] V. Romaka, P. Rogl, L. Romaka, Y. Stadnyk, A. Grytsiv, O. Lakh, and V. Krayovskii, *Intermetallics* **35**, 45 (2013).
- [11] H.-H. Xie, J.-L. Mi, L.-P. Hu, N. Lock, M. Chirstensen, C.-G. Fu, B. B. Iversen, X.-B. Zhao, and T.-J. Zhu, *CrystEngComm* **14**, 4467 (2012).
- [12] H. Xie, H. Wang, Y. Pei, C. Fu, X. Liu, G. J. Snyder, X. Zhao, and T. Zhu, *Adv. Funct. Mater.* **23**, 5123 (2013).
- [13] H. Xie, H. Wang, C. Fu, Y. Liu, G. J. Snyder, X. Zhao, and T. Zhu, *Sci. Rep.* **4**, 6888 (2014).
- [14] K. S. Kim, Y.-M. Kim, H. Mun, J. Kim, J. Park, A. Y. Borisevich, K. H. Lee, and S. W. Kim, *Adv. Mater.* **29**, 1702091 (2017).
- [15] G. Rogl, K. Yubuta, V. Romaka, H. Michor, E. Schafner, A. Grytsiv, E. Bauer, and P. Rogl, *Acta Mater.* **166**, 466 (2019).
- [16] G. Rogl, P. Sauerstich, Z. Rykavets, V. Romaka, P. Heinrich, B. Hinterleitner, A. Grytsiv, E. Bauer, and P. Rogl, *Acta Mater.* **131**, 336 (2017).
- [17] S. Ouardi, G. H. Fecher, C. Felser, J. Hamrle, K. Postava, and J. Pištora, *Appl. Phys. Lett.* **99**, 211904 (2011).
- [18] K. Mastrorardi, D. Young, C.-C. Wang, P. Khalifah, R. J. Cava, and A. P. Ramirez, *Appl. Phys. Lett.* **74**, 1415 (1999).
- [19] J. Pierre and I. Karla, *J. Magn. Magn. Mater.* **217**, 74 (2000).
- [20] M. J. Winiarski and K. Bilińska, *Intermetallics* **108**, 55 (2019).
- [21] M. J. Winiarski, K. Bilińska, K. Ciesielski, and D. Kaczorowski, *J. Alloys Compd.* **762**, 901 (2018).
- [22] K. Synoradzki, K. Ciesielski, L. Kępiński, and D. Kaczorowski, *Physica B* **536**, 659 (2018).
- [23] K. Synoradzki, K. Ciesielski, and D. Kaczorowski, *Acta Phys. Pol. A* **133**, 691 (2018).
- [24] K. Ciesielski, K. Synoradzki, I. Wolańska, P. Stuglik, and D. Kaczorowski, *Mater. Today: Proceedings* **8**, 562 (2019).
- [25] K. Synoradzki, K. Ciesielski, L. Kępiński, and D. Kaczorowski, *Mater. Today: Proc.* **8**, 567 (2019).
- [26] I. Wolańska, K. Synoradzki, K. Ciesielski, K. Załęski, P. Skokowski, and D. Kaczorowski, *Mater. Chem. Phys.* **227**, 29 (2019).
- [27] K. Synoradzki, K. Ciesielski, I. Veremchuk, H. Borrmann, P. Skokowski, D. Szymański, Y. Grin, and D. Kaczorowski, *Materials* **12**, 1723 (2019).
- [28] K. Ciesielski, D. Gnida, H. Borrmann, R. Ramlau, Y. Prots, D. Szymański, Y. Grin, and D. Kaczorowski, *J. Alloys Compd.* **829**, 154467 (2020).
- [29] J. Rodriguez-Carvajal, *Physica B* **192**, 55 (1993).
- [30] V. K. Pecharsky, Y. V. Pankevich, and O. I. Bodak, *Sov. Phys. Crystallogr.* **28**, 97 (1983).
- [31] R. Marazza, D. Rossi, and R. Ferro, *J. Less-Common Met.* **75**, P25 (1980).
- [32] J. Scientific, *TableCurve 2D: Automated Curve Fitting and Equation Discovery* (Jandel Scientific, San Rafael, CA, 1996).
- [33] T. Harmening, H. Eckert, and R. Pöttgen, *Solid State Sci.* **11**, 900 (2009).
- [34] J. H. Mooji, *Phys. Status Solidi* **17**, 521 (1973).
- [35] T. Faber and J. Ziman, *Philos. Mag.* **11**, 153 (1965).
- [36] P. Cote, *Solid State Commun.* **18**, 1311 (1976).
- [37] P. J. Cote and L. V. Meisel, *Phys. Rev. Lett.* **40**, 1586 (1978).
- [38] U. Mizutani, M. Tanaka, and H. Sato, *J. Phys. F. Met. Phys.* **17**, 131 (1987).
- [39] M. Pollak and B. Shklovskii, *Hopping Transport in Solids* (Elsevier, North Holland, 1991).
- [40] B. L. Altshuler and A. G. Aronov, *Electron-electron Interactions in Disordered Systems* (Elsevier, Amsterdam, 1985).
- [41] D. Gnida, M. Szlowska, P. Swatek, and D. Kaczorowski, *J. Phys.: Condens. Matter* **28**, 435602 (2016).
- [42] P. A. Lee and T. V. Ramakrishnan, *Phys. Rev. B* **26**, 4009 (1982).
- [43] J. Kondo, *Prog. Theor. Phys.* **32**, 37 (1964).
- [44] H. Fukuyama, *J. Phys. Soc. Jpn.* **55**, 2118 (1986).
- [45] B. Altshuler, A. Aronov, and A. Zuzin, *Solid State Commun.* **44**, 137 (1982).

- [46] E. Abrahams, P. W. Anderson, D. C. Licciardello, and T. V. Ramakrishnan, *Phys. Rev. Lett.* **42**, 673 (1979).
- [47] B. J. Hickey, D. Greig, and M. A. Howson, *J. Phys. F: Met. Phys.* **16**, L13 (1986).
- [48] J. J. Lin and J. B. Bird, *J. Phys.: Condens. Matter* **14**, 501 (2002).
- [49] Y. Isawa, *J. Phys. Soc. Jpn.* **53**, 2865 (1984).
- [50] A. Sergeev and V. Mitin, *Phys. Rev. B* **61**, 6041 (2000).
- [51] S. Ögüt and K. M. Rabe, *Phys. Rev. B* **51**, 10443 (1995).
- [52] A. M. Jayannavar and N. Kumar, *Phys. Rev. B* **37**, 573 (1988).
- [53] S. Ciuchi, D. D. Sante, V. Dobrosavljević, and S. Fratini, *npj Quantum Mater.* **3**, 44 (2018).